Magnetic force gradient mapping

Tilman E. Schäffer[a)]
Center for Nanotechnology and Institute of Physics, Westfälische Wilhelms-Universitt Münster, Gievenbecker Weg 11, 48149 Münster, Germany

Manfred Radmacher
Institute of Biophysics, University of Bremen, Otto Hahn Allee, 28334 Bremen, Germany

Roger Proksch
Asylum Research Corp., 341 Bollay Drive, Santa Barbara, California 93117

(Received 6 June 2003; accepted 12 September 2003)

Motivated by the difficulty of obtaining quantitative micromagnetic results using current magnetic force microscope imaging techniques, we have employed an imaging mode where the oscillation amplitude of the tip was recorded versus the tip–sample separation as the tip was raster scanned over a magneto-optic sample. The mechanical response of the cantilever depends on the magnetic, but also on topographic, interferometric and nonmagnetic dissipative interactions between the tip and the sample. We separated the magnetic signal from the other interactions and analyzed it in terms of a refined theory of magnetic force microscope response. The extracted magnetic signal, which we refer to as a force gradient map, showed some features not apparent in conventional magnetic force microscope images and was well fit by a simple micromagnetic model of the magneto-optic sample. © *2003 American Institute of Physics.* [DOI: 10.1063/1.1623926]

I. INTRODUCTION

A common application of noncontact, ac-mode force microscopy has been in the study of long-range electrostatic[1] and magnetic[2–4] forces. Conventional noncontact microscopy and tapping mode techniques have been hybridized into a two pass technique termed tapping/lift mode,[5] which provides a means of simultaneously imaging both the sample topography and associated long-range forces. In tapping/lift mode, an initial scan line measures the surface topography. The same scan line is repeated at a constant distance above the topographical features measured during the first scan. In this second pass, the tip is primarily sensitive to the weak but long-range electromagnetic forces. This technique has proven to be very useful in studies of electrostatic[6,7] and magnetic samples,[8–11] but there are a number of problems associated with interpretation of magnetic force microscopy (MFM) images. The following does not present an exhaustive list but includes issues that this work will address.

A magnetic cantilever tip is sensitive to magnetic force gradients, but the quantity of interest in many cases is the sample magnetization. Fundamentally, a consequence of one of Maxwell's equations ($\nabla \cdot \mathbf{B} = 0$) is that a body with a magnetization distribution having a zero divergence, $\nabla \cdot \mathbf{M} = 0$, does not change the measured magnetic field outside of the body. Not surprisingly, even magnetization distributions that differ by a term with a nonzero divergence can look the same to an external observer making a finite number of measurements. Moreover, it can be shown mathematically that, in general, it is impossible to uniquely determine the sample magnetization from MFM measurements.[12] In the special case of a perpendicular sample magnetization, however, the magnetization can theoretically be determined up to a constant.[13] In any case, the tip magnetization is as much a mystery as is the sample magnetization which further complicates the analysis. Interpretation of MFM results in terms of the sample magnetization must necessarily involve some sort of inverse modeling process where a number of micromagnetic and geometrical parameters of the sample and tip are iteratively optimized until the model agrees with the experimental image. As we shall show below, significantly different models can provide reasonable agreement with the same experimental MFM data. It was mathematically shown that acquiring additional MFM images at different scanning heights does not, in theory, provide any additional information about the stray field from the sample.[12] In practice, we found, however, that we could eliminate possible magnetic models by taking measurements at different heights. The reason for this is that the signal-to-noise ratio of a single MFM image at a given height is usually too low for predicting the stray field at other heights.

Another set of problems arises because, in addition to the magnetic forces of interest, the cantilever tip in an MFM experiences nonmagnetic interactions with the sample. These include short-range topographic forces, long-range dissipative effects, and apparent deflections which are artifacts of the optical detection used to observe the cantilever position. Interpretation of MFM images depends on a detailed understanding of how the cantilever dynamics is affected by both magnetic and other, nonmagnetic, interactions. In MFM images taken without tapping/lift mode, the data are acquired at one, approximately constant, height. Therefore, both magnetic and nonmagnetic interactions are imaged together. This has made interpretation of the MFM response quite difficult. One of the main problems separating topography and long-range interactions has been resolved by tapping/lift mode,

a)Electronic mail: tilman.schaeffer@uni-muenster.de

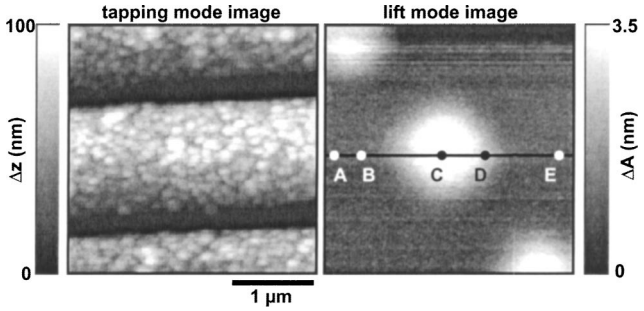

FIG. 1. (a) Topography and (b) magnetic signal (amplitude change) of a magnetic bit on a commercially available magneto-optic disk. The tapping mode image (a) was made in constant amplitude mode. The lift mode image (b) was made at a lift height of 100 nm above the surface. The points labeled A–E are the locations of specific amplitude vs height curves used to discuss our method for separating the magnetic signal from interferometric, short-range topographic, and nonmagnetic dissipative effects.

where data are acquired at two different values of the tip–sample separation. Unfortunately, tapping/lift mode, although extremely good at producing images with magnetic contrast, does not address separating magnetic and nonmagnetic long-range interactions.

Other scanning probe microscopies, such as the scanning tunneling microscope, can be operated in a spectroscopic mode where the bias voltage is ramped while the tunneling current is monitored. This idea has been extended to the atomic force microscope (AFM). A ''force map'' [14–17] is obtained by acquiring the deflection of the cantilever versus the tip–sample separation as a function of the lateral position of the tip. We have applied this technique to noncontact ac-mode force microscopy by acquiring the cantilever oscillation amplitude versus the tip–sample separation and as a function of the lateral position of the tip.[18,19] As the tip–sample separation is varied, damping due to the presence of the surface, laser interference effects, as well as the long-range magnetic signal, affect the measured cantilever oscillation amplitude. We will describe a simple phenomenological procedure for removing the effects of dissipation and variations in the detector sensitivity due to laser interference. This procedure yields the separated magnetic signal which can be analyzed in terms of the tip and sample micromagnetic structure.

II. DATA ACQUISITION

A magnetooptic disk was imaged in the tapping/lift mode (Fig. 1).[20] The tapping mode image [Fig. 1(a)] shows the sample topography. The lift mode image [Fig. 1(b)] shows the associated noncontact image. The amplitude setpoint during the tapping mode image was 55 nm. The ''free'' cantilever oscillation amplitude 3 μm away from the surface was $A_0 \approx 70$ nm. During the ''lift'' part of the scan, the tip–sample separation was set to $z = 100$ nm. We used a commercially available, 225 μm long silicon diving-board-shaped cantilever,[21] coated with 100 nm of CoCr alloy to make it magnetically active.[22] Its resonance frequency was $f_0 = 73.7$ kHz and its spring constant was determined as $k = 1.5$ N/m using the Cleveland method.[23] Prior to imaging, it was magnetized parallel to the z axis in a magnetic field of ≈ 1 T. The coercive field of the tip parallel to the z axis was $\approx 250-290$ Oe.[24] The detection technique used in this work was the ''slope detection'' method where the cantilever is driven at a frequency that maximizes the change in the cantilever oscillation amplitude due to a magnetic response. We recorded an amplitude spectrum of the cantilever in the absence of a sample and chose the drive frequency, $f_D = 73.47$ kHz, at the point where the slope of the resonance curve, $\partial A/\partial f$, was the steepest.

Amplitude curves were acquired by recording the cantilever oscillation amplitude as a function of the z piezovoltage which was ramped. To generate an ''amplitude map,'' the sample was slowly raster scanned in the x and y directions while the z scans were being made. Thus, an amplitude map is a three-dimensional map of the oscillation amplitude of the tip over the sample. The amplitude curves were recorded using modified Nanoscope III electronics (VEECO, Santa Barbara, CA). The Nanoscope itself was only used for generating the scan voltages in the x and y directions. The z piezo was driven by analog electronics using a function generator biased by a high precision dc power supply without feedback. The data were recorded on a separate computer, equipped with custom data acquisition hardware and software. The data were then processed to separate the magnetic signal from other effects (discussed below). The separate electronics could be bypassed so that the z voltage was controlled by the Nanoscope again, thus making it possible to acquire conventional tapping/lift mode images.

Z scans of 670 nm range were made at 4–50 Hz. The amplitude as a function of the z piezovoltage was sampled at 100 points during both the approach and retraction. Because of the slow z scan rate, usually only 128 amplitude curves per line were recorded, resulting in lateral line scan rates of 0.1–0.5 Hz. Although we recorded three-dimensional amplitude datasets, $A(x,y,z)$, in the analysis below, we will discuss vertical slices $A(x,y=\text{constant},z)$.

It might be possible to acquire the same data using tapping/lift mode by simply taking lift mode images at a variety of z values. However, there are a number of advantages to the technique used in this work. Because tapping/lift mode requires two passes for each image, the resulting data acquisition takes twice as long. On the Nanoscope, we observed that this increase in time often resulted in significant lateral drift between the beginning and end of the imaging process. This drift makes the alignment of the subsequent images difficult, especially since the height of each lift mode image varies within the image. We also found that operating in lift mode with a height of less than 50 nm sometimes resulted in the lift mode image becoming unstable, presumably because of unwanted contact with the surface (''tip crashes''). This may have been because of creep or hysteresis in the scanning piezo in the time between the tapping scan and the subsequent lift scan. All three of these problems are eliminated with force gradient maps.

III. EXTRACTING THE MAGNETIC SIGNAL

Typical amplitude versus z piezovoltage curves taken on and around the central magnetooptic bit of Fig. 1 are shown

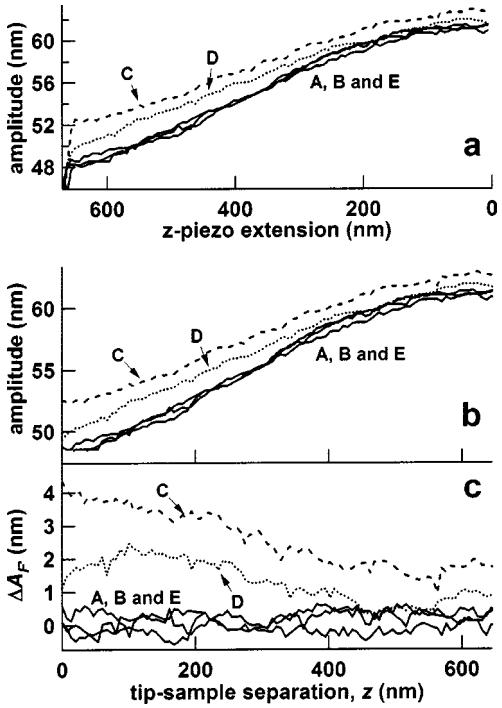

FIG. 2. Illustration of the method for extracting the force gradients from the other apparent and real effects the cantilever experiences. (a) Cantilever oscillation amplitude vs z-piezo extension. Traces C and D are made over the magneto-optic bit, traces A, B, and E are taken away from it (see Fig. 1). All traces exhibit a sharp change in slope where the cantilever first starts to tap the surface of the sample ($z \approx 650$ nm). If the amplitude setpoint during a regular tapping mode image was substantially less than the amplitude at this discontinuity, then the respective image would primarily be of topographic origin (tapping mode). The magnetic interactions between the tip and the magneto-optic bit are primarily attractive in this measurement, shifting the resonant frequency of the cantilever down. Because the cantilever is being driven below its resonance, this results in an increase of the cantilever amplitude over the bit (C and D) relative to the periphery (A, B, and E). The free cantilever oscillation amplitude was $A_0 = 62$ nm. (b) Cantilever oscillation amplitude after the data to the left-hand side of the slope discontinuity were removed and the curves were realigned with the $z = 0$ vertical axis. The horizontal scale now more accurately reflects the tip–sample separation, z. Curves A, B, and E contain the nonmagnetic dissipative and interferometric effects while C and D show a magnetic interaction as well. (c) Cantilever oscillation amplitude after subtraction of the average of all curves in the force gradient map that are away from the bit. The nonmagnetic dissipative, the interferometric, and the topographic effects are now eliminated. Therefore, curves A, B, and E are roughly zero while C and D are assumed to only contain magnetic information. Such curves were used to produce the gray-scale images in Fig. 3.

in Fig. 2(a). Note that the curves taken over positions C and D are significantly different from the ones taken farther away from it (A, B, and E). It is also important to note that the curves taken away from the bit lie on top of each other. This behavior will be exploited in the following section to extract the magnetic signal from the topographical, interferometric, and dissipative parts of the signal.

The short-range topographical interactions between the tip and sample were the simplest to handle in our analysis. Whatever the origin of the topographical forces, their result was a sudden apparently discontinuous change in the slope of the amplitude curves. We used this sudden change in slope to define the surface of the sample. For the particular amplitude curves here, data were acquired at 6.7 nm intervals. On this scale, the transition from noncontact (off surface) to tapping (on surface) is relatively sharp and we can view the slope in this transition region as changing discontinuously. The topographical effects were consequently removed by simply discarding the data points to the left-hand side of this discontinuous change in slope and realigning the data with the left-hand ($z = 0$) axis. This process defines the sample surface ($z = 0$) for each amplitude curve. This transformation of the data is apparent in the shifting of the amplitude curves [Fig. 2(a)] to the left-hand side [Fig. 2(b)].

The remaining noncontact data contain dissipative, interferometric as well as magnetic information. The tip and sample were both grounded to eliminate electrostatic forces.[25] Other interactions, like van der Waals interactions, which are of much shorter range than the magnetic interactions, were neglected. Also, we checked the sample for dissipative magnetic interactions[26] and found none.

Interferometric effects are caused by the optical detection of cantilever deflections.[27,28] When working with reflective samples, stray reflections from the sample surface interfere with the reflection from the cantilever, causing apparent cantilever motion. When the AFM is operated in a conventional scanning mode and the scan size is much smaller than the laser spot size, interference effects are generally constant over the scan field. When operating in the force mapping mode, however, the tip–sample separation is continuously changing, resulting in interference effects which often appear as periodic oscillations in the amplitude curves.

Dissipative effects are due to the mechanical damping of the cantilever motion, as there is usually a significant damping effect when an oscillating cantilever approaches a surface, due to hydrodynamic squeeze-film damping between the cantilever and the sample.[29]

We will make the simplest assumption that the changes in cantilever oscillation amplitude due to these effects are independent of each other. This allowed the dissipative and interferometric effects to be subtracted from the amplitude curves to yield the magnetic contribution. As evident from the overlapping of the force curves from nonbit areas [Fig. 2(b)], both dissipative and interferometric effects did not depend on the lateral position of the cantilever. Our procedure therefore was to average several amplitude curves from nonbit areas of the sample to get the laterally independent interferometric and dissipative contribution to the amplitude, and to subtract that average from each amplitude curve in the amplitude map to obtain the (conservative) magnetic contribution to the cantilever amplitude [Fig. 2(c)].

The presence of a magnetic force gradient in the z direction, F_z', which the tip experiences during its oscillation, shifts the resonant frequency of the cantilever. For slope detection, this shift is proportional to the measured change in amplitude $\Delta A_{F'}$:

$$\Delta f_{F'} = -\left(\left. \frac{\partial A}{\partial f} \right|_{f_D} \right)^{-1} \Delta A_{F'} . \tag{1}$$

The slope of the resonant curve at the drive frequency, $\partial A / \partial f |_{f_D}$, represents the sensitivity of the detection and varies with the tip–sample separation, z, mostly because the

damping increases when the tip approaches the sample surface.[29] We measured this dependence on z by acquiring amplitude curves at different frequencies around f_D and taking the numerical derivative with respect to f. For the data shown in this work, we found a nearly linear dependence of the slope on z. The effect was significant, typically decreasing the slope by about 20% from $z=670$ nm to the ''contact'' point at $z=0$ nm. This effect of decreasing sensitivity as z decreased was accounted for in the conversion of the data from amplitude change to resonant frequency shift.

Converting the resonant frequency shift of the cantilever at a certain position into the experienced force gradient at that position is complex, since the tip oscillation cannot be treated in the small amplitude limit. Instead, it experiences a varying force gradient along its oscillatory trajectory. Following the work of Dürig,[30,31] we define an ''effective force gradient,'' $F'_{z,\mathrm{eff}}$ [sign convention see Fig. 4(a)]:

$$F'_{z,\mathrm{eff}} = -\frac{2k}{f_0}\Delta f_{F'}\,. \tag{2}$$

Note that in the special case of a purely harmonic interaction force, the ''effective'' force gradient becomes the ''true'' force gradient. We refer to the resulting data (force gradient as a function of vertical and lateral position) as an (effective) force gradient map. Vertical slices of force gradient maps over the magneto-optic bit are displayed as grayscale images [Figs. 3(a)–3(d)]. The force gradient maps were acquired with $A_0=21$, 40, 62, and 190 nm for Figs. 3(a)–3(d), respectively. An increase in the signal-to-noise ratio for increasing A_0 is apparent in the image series. The images in Fig. 3 demonstrate that it is also important to consider the oscillatory movement of the tip during the imaging process and reconfirm that the small amplitude limit is not applicable here.

IV. MODELING THE MAGNETIC FORCE MICROSCOPY RESPONSE

To calculate the MFM amplitude response for our models from Eq. (2), it is necessary to calculate the force gradient acting between tip and sample.[32] It is possible to do this by utilizing Fourier-based methods.[33,13] Here we will, however, work in direct space. With the assumption that both sample and tip coating consist of a magnetic material hard enough so that their magnetizations do not affect each other,[34] the force gradient (in the z direction) experienced by the tip can be calculated by integrating the second derivative of the z component of the magnetic field from the sample with respect to z over the volume of the tip coating:[4,35]

$$F'_z(\mathbf{r}) = \mu_0 M_{\mathrm{tip}} \int_{\mathrm{tip}} \frac{\partial^2 \mathbf{H}_z(\mathbf{r}+\mathbf{s}')}{\partial z^2}\, dV', \tag{3}$$

where $\mathbf{r}$ is the position of the tip origin with respect to the sample origin [Fig. 4(a)]. $\mathbf{s}$ denotes the position of a volume element in the tip relative to the tip origin. We assumed that the tip magnetization, M_{tip}, is single domain and is oriented in the z direction. This assumption is good for typical MFM tips.[36] (Alternatively, integration over the induced magnetic surfaces charges could have been performed, decreasing the dimensionality of the integral.) In the long run, it would be desirable to include the possibility of the micromagnetic structure of the tip and sample modifying each other.[37] For the data presented here, however, the absence of hysteretic dissipation effects suggests that the sample and tip magnetization do not significantly affect each other. This is further supported by the fact that both the magnetic tip and the sample have relatively high coercive fields.[24]

Equation (3) is sufficient in the limit of small tip oscil-

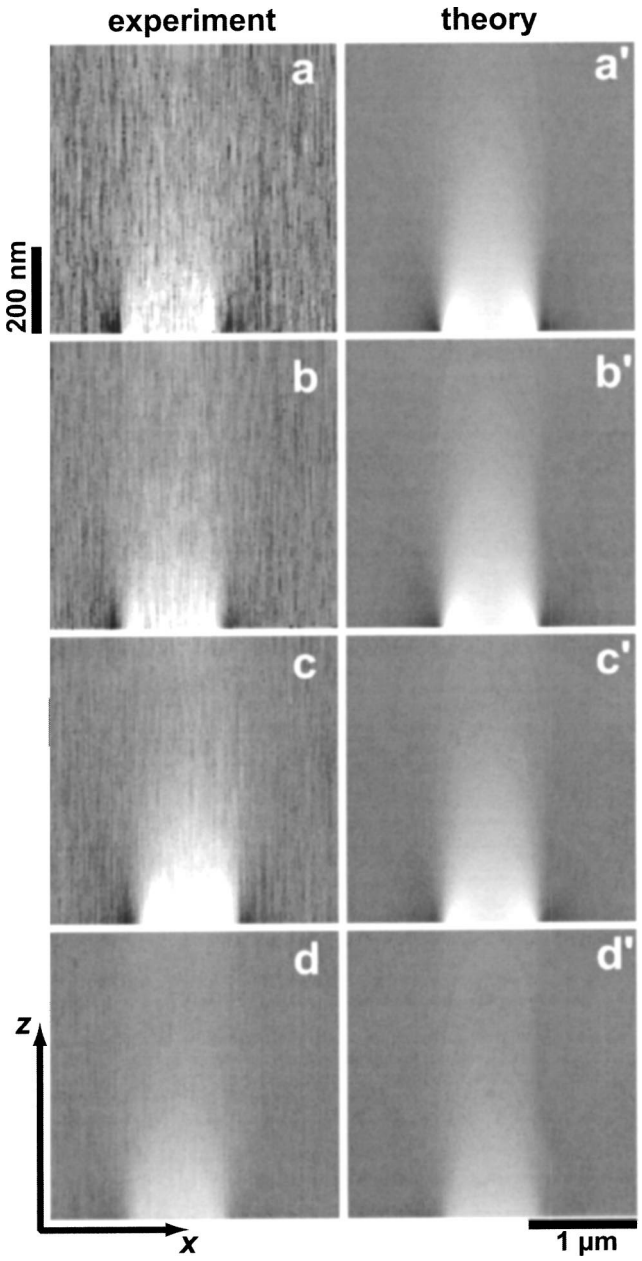

FIG. 3. Experimental and theoretical grayscale images of the extracted magnetic response over the magneto-optic bit. The grayscale corresponds to changes in the effective magnetic force gradient as a function of the lateral and horizontal position of the tip. The experimental free cantilever oscillation amplitudes (A_0) were 21, 40, 62, and 190 nm for (a)–(d), respectively. Theoretical images calculated for the uniformly magnetized finite cylinder (double disk) model [(a)–(d)], closely reproduce the experimental data. The grayscale range of all images in the left-hand side column (and that of all images in the right-hand side column, respectively) was chosen to be identical.

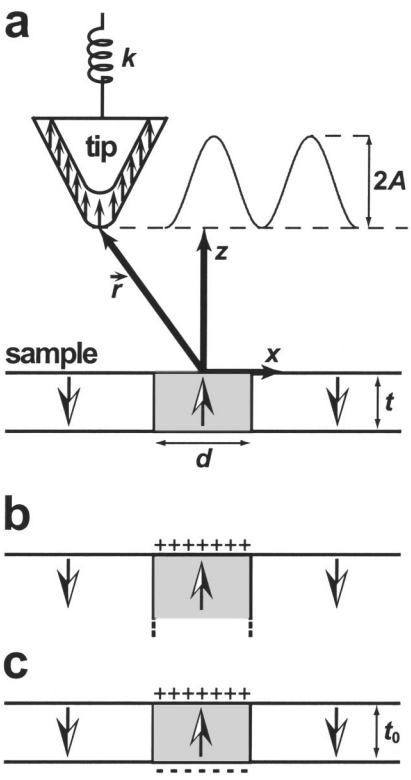

FIG. 4. Schematic of the theoretical models used. (a) The tip was modeled as a cone with its symmetry axis in z direction, 10 μm in height, with an opening angle of 17°, a spherical cap of radius 10 nm and a 100 nm thick magnetic coating that was completely magnetized along the z axis. (b) First magnetostatic model of the sample, representing the magneto-optic bit as a uniformly magnetized 1 μm diameter half-infinite cylinder in an oppositely magnetized half-infinite volume (single disk model). (c) Second magnetostatic model of the sample, representing the magneto-optic bit as a uniformly magnetized cylinder, 1 μm in diameter, and 50 nm in thickness, placed in an infinite film of the same thickness that is uniformly magnetized in the opposite direction (double disk model).

lation amplitudes. However, as discussed above, there can be a significant dependence of the measurement signal on the cantilever oscillation amplitude. Among others,[38,39] this problem has been addressed by Dürig.[30,31] In the limit of a weak tip–sample interaction such that the motion of the tip is essentially harmonic, the effective force gradient, as defined in Eq. (2), can be written as a convolution product,[31]

$$F'_{z,\mathrm{eff}}(x,y,z) = -\frac{2}{\pi A^2}\int_z^{z+2A} F_z(x,y,z') \times g_1\left(\frac{z'-z}{A}-1\right)dz', \tag{4}$$

with a weakly diverging kernel

$$g_1(u) = -\frac{u}{\sqrt{1-u^2}}. \tag{5}$$

By applying partial integration to Eq. (4), we find

$$F'_{z,\mathrm{eff}}(x,y,z) = \frac{2}{\pi A}\int_z^{z+2A} F'_z(x,y,z')\, g_2\left(\frac{z'-z}{A}-1\right)dz', \tag{6}$$

with a nondiverging kernel

$$g_2(u) = \sqrt{1-u^2}. \tag{7}$$

Due to the harmonic nature of the tip oscillation, $g_2[(z'-z)/A-1]$ is proportional to the tip velocity at each tip position z'. Therefore, Eq. (6) obtains the effective force gradient by weighting the force gradient at each position with the corresponding tip velocity and by calculating the average over the oscillation range. The contribution of the force gradient to the effective (=weighted and averaged) force gradient is highest at the respective static equilibrium position of the tip (where the tip velocity is highest) and is lowest (zero) at the respective points of maximum/minimum tip extension.

We modeled the sample as an infinitely extended film of thickness t and uniform magnetization in z direction, in which a magneto-optic bit of opposite magnetization, M_{bit}, is embedded in the shape of a cylinder of diameter $d = 1\ \mu$m and thickness t (perpendicularly magnetized medium) [Fig. 4(a)]. The magnetic field above an infinitely extended and uniformly magnetized film vanishes. Therefore, the relevant magnetic field (''stray field'') of our sample model is effectively created by an isolated magnetic bit having an effective magnetization of $2M_{\mathrm{bit}}$. (Besides, MFM measurements are insensitive to homogenous magnetic fields.) There are no moving charges in the sample, so one can define a scalar magnetic potential und subsequently reduce the problem to that of two charged disks, one at the top surface (+) and one at the bottom surface (−) of the bit, each with a magnetic surface charge density of[40]

$$\sigma_{\pm} = \pm 2M_{\mathrm{bit}}. \tag{8}$$

The magnetic field of the two charged disks becomes[40]

$$\mathbf{H}(\mathbf{r}) = \frac{1}{4\pi}\int_{\mathrm{sample}} \sigma_{\pm}\frac{\mathbf{r}-\mathbf{r}'}{|\mathbf{r}-\mathbf{r}'|^3}dS', \tag{9}$$

where the integral is to be performed over the top and the bottom surface of the disk.

Our first model represents a magnetic film of infinite thickness [Fig. 4(b)], therefore, the magnetic field of the bottom disk vanishes and we have to consider a single disk (the top one) only. Relevant for our MFM measurements is the z component of $\mathbf{H}$ in the xz plane (the center of the disk is assumed at the origin of the coordinate system, $\mathbf{r}=0$). H_z can be expressed in cylindrical coordinates:

$$H_z^{\mathrm{single}}(x,z) = \frac{M_{\mathrm{bit}}}{2\pi}\int_0^{2\pi} d\varphi \times \int_0^R \frac{zr}{(x^2+z^2+r^2-2xr\cos\varphi)^{3/2}}dr. \tag{10}$$

Our second model represents a uniformly magnetized cylinder of a typical film thickness of $t_0 = 50$ nm, the magnetic field of which is that of two oppositely charged single disks, separated by t_0 [Fig. 4(c)]:

$$H_z^{\mathrm{double}}(x,z) = H_z^{\mathrm{single}}(x,z) - H_z^{\mathrm{single}}(x,z+t_0). \tag{11}$$

For both sample models, the tip was modeled[4] as a truncated cone, 10 μm in height, with an opening half-angle of 17°,

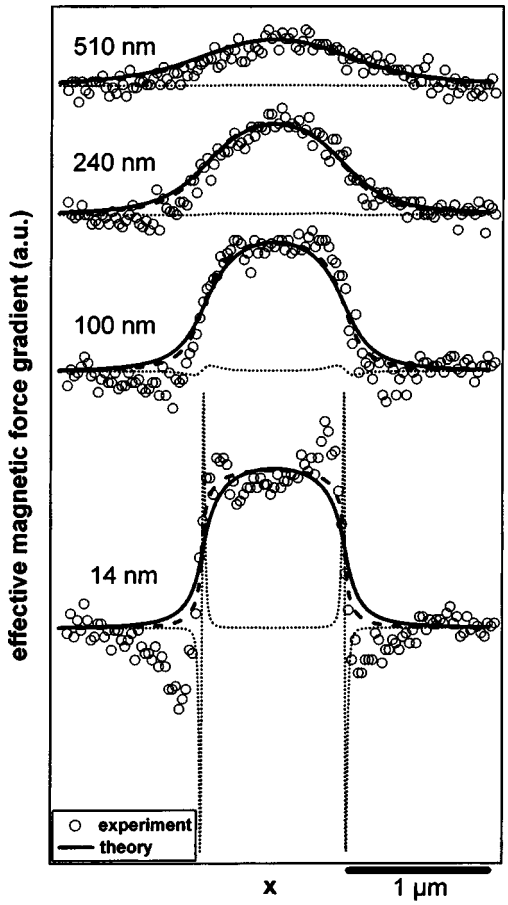

FIG. 5. Comparison of the experimental force gradient map data with the single disk model for four different tip–sample separations ($A_0 = 62$ nm). Traces from the tip model with (solid lines) and without (dashed lines) considering large-amplitude effects were fit to the experimental data simultaneously. At large values of z, the fits seem reasonable but as the MFM tip begins to sample the magnetic near field ($z = 14$ nm), the fits clearly begin to disagree with the data. Clearly, a point dipole model (zero-tip size, small oscillation amplitude) (dotted lines) does not reproduce the data at all.

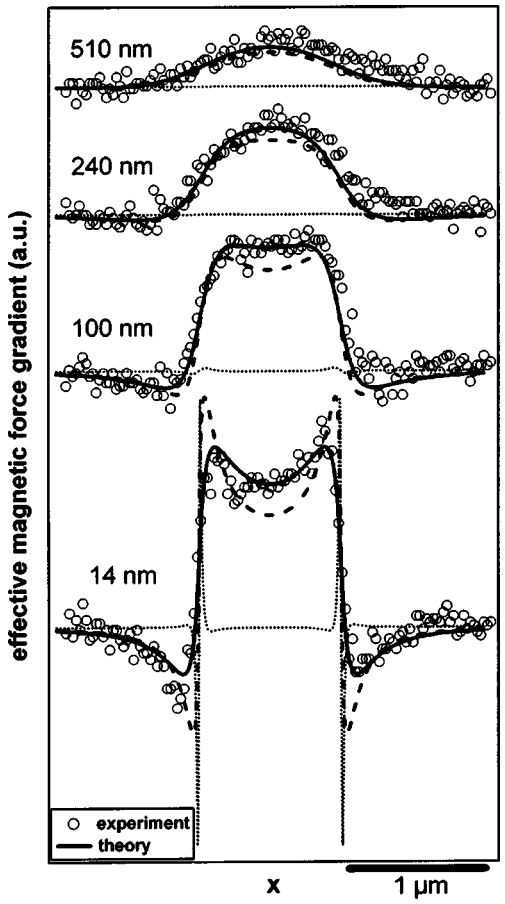

FIG. 6. Comparison of the experimental force gradient map data with the double disk model for four different tip–sample separations ($A_0 = 62$ nm). Traces from the tip model with (solid lines) and without (dashed lines) considering large-amplitude effects were fit to the experimental data simultaneously. A good fit is obtained for the full-grown tip model (solid lines), where the features of the experimental data are faithfully reproduced on all the length scales recorded. Again, a point dipole model (dotted lines) does not reproduce the data at all.

and a spherical cap at the tip apex of radius 10 nm. The opening angle was approximated by scanning electron microscopy and the tip radius was estimated from the specifications of the manufacturer. Increasing the cone height in the tip model to more than 10 μm did not significantly change the results. Since we were only interested in qualitative comparisons of the MFM responses, we left the saturation magnetization of the tip coating, M_{tip}, as a linear fitting parameter.

V. RESULTS AND DISCUSSION

To compare the quality of both sample models, we selected four lateral traces at different tip heights from the experimental force gradient map shown in Fig. 3(c) (oscillation amplitude 62 nm) (Figs. 5 and 6, markers). Then, we calculated the theoretical traces resulting from the two different sample models: The single disk model (Fig. 5, solid lines), and the double disk model (Fig. 6, solid line). All four theoretical traces were least-square fit to the four respective experimental curves simultaneously, with the tip magnetization and the x offset as global fitting parameters (i.e., the same value for all traces). The trace at $z = 14$ nm (Fig. 5) shows the main discrepancy between the data and the single disk model: The fine structure on the edge of the bit is completely missing from the calculated trace. Despite this discrepancy, the theoretical traces fit reasonably well to the experimental traces at larger values of z. The calculated traces of the double disk model (Fig. 6) fit the data much better at all values of z, especially in the near field (when z is comparable to the media thickness). The slight asymmetry in the data (a lower dip on the left-hand side of the bit and a higher peak on its right-hand side) is probably due to the fact that the tip axis is tilted with respect to the vertical ($\approx 10°$) in the experiment but not in the theory.

As a demonstration that both the steps of (a) integrating over the volume of the tip coating [Eq. (3)] and (b) correcting for the large-amplitude tip oscillation [Eq. (6)] are necessary in the modeling, we also plotted the theoretical traces without the large-amplitude correction (Figs. 5 and 6, dashed lines), and without both the large-amplitude correction and the tip volume correction (point dipole tip model, Figs. 5 and 6, dotted lines). The latter traces clearly do not fit the data for both sample models.[41] The former traces track the basic

shape of the experimental traces. But a faithful reproduction of the features of the experimental traces was only obtained for the double disk sample model, using the full-grown tip model (Fig. 6, solid lines). Such a fit had a chi-square that was smaller by a factor of 2.5 than that from the single disk model. The results from the other data sets ($A_0 = 21$, 40, and 190 nm, respectively) were similar. Therefore, the double disk model is a more likely model of the true sample magnetization.

This analysis emphasizes the importance of examining different length scales of the micromagnetic structure by sampling and modeling the MFM response at different values of z. If there is a micromagnetic structure with a characteristic length ℓ, it is necessary for the MFM to operate in the near field ($z \lesssim \ell$) to resolve the structure. In the case of the magneto-optic bit studied in this work, there were two length scales we were able to study, the diameter of the bit ($\approx 1\ \mu$m) and the thickness of the media (≈ 50 nm). The diameter of the bit was clearly resolved and had approximately the same value in all of the measurements in Figs. 5 and 6. If we had a sufficient signal-to-noise ratio to probe $z > 1\ \mu$m, we would certainly see the apparent diameter of the bit begin to grow. Moving in closer to the sample, the finite media thickness became apparent only as z went below ≈ 50 nm. For this reason, conventional MFM images that are usually acquired at a lift height of above 50 nm are not well suited to discriminate between different magnetic sample models. These effects are also visible in the experimental data shown in Figs. 3(a)–3(d). The complete set of calculated magnetic response for the double disk model is shown in the grayscale images of Figs. 3(a)′–3(d)′, which are in good agreement with the experimental data.

VI. CONCLUSION

We have presented a way of acquiring and displaying images of magnetic information that is complementary to existing techniques. Force gradient maps provide a unique and powerful way of displaying information about long-range forces. By taking multiple amplitude curves, it is possible to separate the effective magnetic force gradient from other effects. When we applied this technique to magneto-optic bits, we found that the MFM response could be more accurately modeled if the effect of the finite oscillation range of the tip on the effective magnetic force gradient was considered. The theoretical response of the MFM to a magneto-optic bit was calculated assuming two simple models: (a) A half-infinite uniformly magnetized cylinder (''single disk'') and (b) a uniformly magnetized cylinder 50 nm thick (''double disk''). While conventional MFM images at a larger lift height could be reproduced by both models by constraining the MFM signal dependence of the tip–sample separation, the force gradient map showed that the double disk model provided a better description of the MFM response. These results highlight the importance of considering the various length scales involved in MFM measurements when interpreting magnetic images.

ACKNOWLEDGMENTS

The authors are grateful to Harald Fuchs and Paul Hansma for discussions and to André Schirmeisen und Boris Anczykowski for a critical reading of the manuscript.

[1] Y. Martin, D. W. Abraham, and H. K. Wickramasinghe, Appl. Phys. Lett. **52**, 1103 (1988).
[2] Y. Martin and H. K. Wickramasinghe, Appl. Phys. Lett. **50**, 1455 (1987).
[3] P. Grütter, H. J. Mamin and D. Rugar, *Magnetic Force Microscopy* (Springer, Berlin, 1992), pp. 151–207.
[4] D. Rugar, H. J. Mamin, P. Guenther, S. E. Lambert, J. E. Stern, I. McFayden, and T. Yogi, J. Appl. Phys. **68**, 1169 (1990).
[5] Implemented on the Nanoscope III from Digital Instruments, Santa Barbara, CA.
[6] K. M. Jones, P. Visconti, F. Yun, A. A. Baski, and H. Morkoc, Appl. Phys. Lett. **78**, 2497 (2001).
[7] H. Q. Ni, Y. F. Lu, Z. Y. Liu, H. Qiu, W. J. Wang, Z. M. Ren, S. K. Chow, and Y. X. Jie, Appl. Phys. Lett. **79**, 812 (2001).
[8] E. D. Dahlberg and J. G. Zhu, Phys. Today **48**, 34 (1995).
[9] R. Proksch, S. Foss, and E. D. Dahlberg, IEEE Trans. Magn. **30**, 4467 (1994).
[10] W. Rave, L. Belliard, M. Labrune, A. Thiaville, and J. Miltat, IEEE Trans. Magn. **30**, 4473 (1994).
[11] E. B. Svedberg, S. Khizroev, C. H. Chang, and D. Litvinov, J. Appl. Phys. **92**, 6714 (2002).
[12] B. Vellekoop, L. Abelmann, S. Porthun, and C. Lodder, J. Magn. Magn. Mater. **190**, 148 (1998).
[13] H. J. Hug, B. Stiefel, P. J. A. van Schendel, A. Moser, R. Hofer, H.-J. Güntherodt, S. Porthun, L. Abelmann, J. C. Lodder, G. Bochi, and R. C. O'Handy, J. Appl. Phys. **83**, 5609 (1998).
[14] C. M. Mate, M. R. Lorentz, and V. J. Novotny, J. Chem. Phys. **90**, 7550 (1989).
[15] M. Radmacher, J. P. Cleveland, M. Fritz, H. G. Hansma, and P. K. Hansma, Biophys. J. **66**, 2159 (1994).
[16] D. R. Baselt and J. D. Baldeschwieler, J. Appl. Phys. **76**, 33 (1994).
[17] K. O. v. d. Werf, C. A. J. Putman, and J. G. G. d. Grooth, Appl. Phys. Lett. **65**, 1195 (1994).
[18] M. A. Lantz, H. J. Hug, R. Hoffmann, P. J. A. van Schendel, P. Kappenberger, S. Martin, A. Baratoff, and H.-J. Güntherodt, Science **291**, 2580 (2001).
[19] H. Hölscher, S. M. Langkat, A. Schwarz, and R. Wiesendanger, Appl. Phys. Lett. **81**, 4428 (2002).
[20] 1 GB Rewriteable, Imation Corp., St. Paul, MN.
[21] NanoWorld Services, Wetzlar, Germany.
[22] Coated by Advanced Research, Minneapolis, MN.
[23] J. P. Cleveland, S. Manne, D. Bocek, and P. K. Hansma, Rev. Sci. Instrum. **64**, 403 (1993).
[24] K. L. Babcock, V. B. Elings, J. Shi, D. D. Awschalom, and M. Dugas, Appl. Phys. Lett. **69**, 705 (1996).
[25] We assumed that there were no pinned charges as the sample was a fairly good conductor.
[26] R. Proksch, K. Babcock, and J. P. Cleveland, Appl. Phys. Lett. **74**, 419 (1999).
[27] G. Meyer and N. M. Amer, Appl. Phys. Lett. **53**, 1045 (1988).
[28] S. Alexander, L. Hellemans, O. Marti, J. Schneir, V. Elings, P. K. Hansma, M. Longmire, and J. Gurley, J. Appl. Phys. **65**, 164 (1989).
[29] F. M. Serry, P. Veuzil, R. Vilasuso, and G. J. Maclay, *Proceedings of the Second International Symposium on Microstructures and Microfabricated Systems*, (Chicago Electrochemical Society, Pennington, NJ, 1995), p. 83.
[30] U. Dürig, Appl. Phys. Lett. **75**, 433 (1999).
[31] U. Dürig, Appl. Phys. Lett. **76**, 1203 (2000).
[32] A stationary cantilever experiencing an static, external force, F, is deflected by $\Delta z = F/k$. During the noncontact portion of the amplitude curves, the largest force we measured was on the order of 1 nN, which caused a static deflection on the order of 1 nm. Since this deflection was much smaller than the 6.7 nm steps taken in the amplitude curves, we neglected static forces on the cantilever.
[33] C. Schönenberger and S. F. Alvarado, Z. Phys. B: Condens. Matter **80**, 373 (1990).
[34] U. Hartmann, J. Appl. Phys. **64**, 1561 (1988).
[35] A. Wadas, P. Grütter, and H.-J. Güntherodt, J. Vac. Sci. Technol. A **8**, 416

(1990).
[36] S. Porthun, L. Abelmann, and C. Lodder, J. Magn. Magn. Mater. **182**, 238 (1998).
[37] D. Abraham and F. A. McDonald, Appl. Phys. Lett. **56**, 1181 (1990).
[38] B. Anczykowski, J. P. Cleveland, D. Krüger, V. Elings, and H. Fuchs, Appl. Phys. A: Mater. Sci. Process. **66**, S885 (1998).
[39] F. J. Giessibl, Phys. Rev. B **56**, 16010 (1997).
[40] J. D. Jackson, *Classical Electrodynamics*, 2nd Ed. (Wiley, New York, 1975).
[41] It is possible, however, to obtain a better fit when the point dipole tip in the model is arbitrarily positioned much farther from the sample surface than the tip apex.